Plasma Chemistry and Plasma Processing (2023) 43:957–974
https://doi.org/10.1007/s11090-023-10346-7

ORIGINAL PAPER

Atmospheric Non-thermal Plasma Reduction of Natively Oxidized Iron Surfaces

Viktor Udachin[1] · Lienhard Wegewitz[1] · Maik Szafarska[1] · Sebastian Dahle[1,2] · René Gustus[1] · Wolfgang Maus-Friedrichs[1]

Received: 1 December 2022 / Accepted: 8 June 2023 / Published online: 17 June 2023

Abstract

Plasma in hydrogen-containing atmospheres is an efficient method for the reduction of iron oxides. Although a vast number of approaches were performed for the reduction of bulk Fe oxides with thermal hydrogen plasmas, there is almost no information about the non-thermal plasma reduction efficiency in the atmospheric pressure range. In the current article we present the reduction of natively oxidized iron surfaces applying a dielectric barrier discharge plasma in an Ar/H_2 atmosphere at 1000 hPa. By varying the surface temperature from 25 to 300 °C, we studied the plasma reduction efficiency, which was then compared with a thermal method. Whereas plasma treatments at 25 °C and 100 °C did not result in the significant reduction of iron oxidized species, experiments at 200 °C and 300 °C yielded a reduction of approximately 88% and 91% of initial oxidized components already after 10 s, respectively. Moreover, we observed an increase in the efficiency with a plasma-thermal reduction in comparison to a thermal method, which was attributed to the presence of atomic hydrogen in the plasma phase. Analysis of morphology revealed the formation of Fe–C structures on surfaces after thermal and plasma-thermal treatments at 200 °C and 300 °C that may be connected with the diffusion of bulk contaminations to the deoxidized surface and reactions between the reduced Fe with plasma-activated adventitious carbon. Conclusively, the plasma was characterized by analyzing the reactive species and the electron temperatures.

Keywords Dielectric barrier discharge · X-ray photoelectron spectroscopy · Iron deoxidation · Argon–hydrogen plasma · Iron oxide reduction

✉ Viktor Udachin
viktor.udachin@tu-clausthal.de

[1] Clausthal Center of Materials Technology, Clausthal University of Technology, Agricolastraße 2, 38678 Clausthal-Zellerfeld, Germany

[2] Department of Wood Science and Technology, Biotechnical Faculty, University of Ljubljana, Jamnikarjeva Ulica 101, 1000 Ljubljana, Slovenia

Introduction

Removal of native oxide layers from metal surfaces is an important treatment step in metal manufacturing processes like coating, welding or bonding, since surface metal oxides usually negatively affect the mechanic or adhesive properties of samples and final products [1–5]. For example, strength and fatigue limit of sintered steels can be improved by reducing the amount of oxygen and surface oxides in the primary Fe samples [1, 2, 4]. In addition, oxidized metal surfaces are known for their poor adhesive properties in comparison to deoxidized ones [6, 7].

Reduction of iron oxides can be successfully performed by thermal hydrogen plasmas [5]. Dissociated and ionized hydrogen gas within the system is found to be effective in the reduction processes. Nevertheless, as the working temperatures of such methods are usually in the range of several thousand Kelvin, they cannot be applied for the deoxidation of metal surfaces, since melting and a strong change of the crystal structure occur [5, 8]. Therefore, development of a method that can be applied for the removal of oxygen species from iron surfaces without significant changes of morphology is of interest.

One promising way of reducing metal surfaces utilizes non-thermal hydrogen plasmas. As it was shown in our previous research, copper surface oxides can be successfully reduced within seconds of treatment, using an Ar/H_2 dielectric barrier discharge plasma (DBD) in the atmospheric pressure range and at room temperature [9]. We attributed the deoxidation effect to the presence of reducing agents like atomic hydrogen in the plasma phase [9]. Thermodynamically more stable metal compounds like iron oxides that form layers on metal, steel or alloy surfaces also can be removed using deoxidation plasma techniques [5]. As it was previously mentioned, thermal plasmas have long been used for the deoxidation of iron melts [5, 10] and the results have been partly transferred towards low-pressure plasmas for the deoxidation of solid items, including historic artefacts [11]. In the review on different hydrogen plasma reduction methods, Sabat and colleagues considered that plasma-enhanced reduction processes provide thermodynamic and kinetic advantages over other methods like for e.g. heating in hydrogen [5, 12]. An increase in efficiency was connected with the presence of vibrationally excited hydrogen molecules as well as ionic and atomic hydrogen within the plasma phases [5, 13]. For example, Rajput and colleagues performed an almost complete reduction of hematite by a microwave (MW) plasma in 5 hPa hydrogen at 300 °C after 120 min [13]. They observed a decline in activation energy of the plasma-enhanced reduction process in comparison to heating in H_2, which was most-likely triggered by vibrationally excited hydrogen molecules [5, 13]. The application of a low-pressure radio-frequency (RF) hydrogen plasma for the removal of 30 nm-thick surface oxide layers on $Fe_{60}Ni_{40}$ substrate was shown by Mozetic and colleagues [14]. They revealed that the surface oxide layer was removed within 20 s of treatment at a surface temperature of approximately 185 °C. The rise of a surface temperature was mainly attributed to the recombination of hydrogen atoms on the surface [5, 14]. Chromium substrates were also reduced in a low pressure microwave plasma at higher efficiencies compared to thermal or heterogeneous reduction [15, 16]. Atomic hydrogen from the reduction process, however, remained interstitially within the material, leading to hydrogen embrittlement. The same effect of the enrichment of atomic hydrogen within a metal surface after plasma deoxidation was also found on iron and steel work pieces [17]. The surface of a stainless steel AISI316L with a 500 nm thick oxide layer was successfully deoxidized in a MW hydrogen plasma at 0.4 hPa. [18]. The reduction process occurred sequentially in a few seconds with reducing of Mn oxides, Fe oxides and Cr oxides. Although the sample

temperature rose to over 1000 °C in the course of the treatment due to the enthalpy of reaction, the energy transferred into the plasma and the additional heating, it was still well below the melting temperature, especially for chromium oxide. In general, non-thermal plasma techniques that operate at low pressures show potential for deoxidation applications [5]. However, these are mostly limited by the complex setups of many of the plasma devices. Interestingly, approaches in atmospheric non-thermal hydrogen plasmas for the reduction of iron surface oxides so far have not been studied at all [5], whereas for other metals like copper, treatments at pressures in the atmospheric pressure range were found to be effective already at room temperature [9]. In addition, the attractiveness of non-thermal plasma techniques for the reduction of metal surfaces include minor impacts on the morphology of sample surfaces as well as the relative simplicity of the setups, which highlights these methods among the known surface oxide reduction approaches [5, 9, 19–21].

In this work, we show the reduction of natively oxidized iron surfaces using a non-thermal DBD plasma at 1000 hPa in a gas mixture of Ar/H_2 with an H_2 content of 2%. DBD plasma treatment of samples was performed at different surface temperatures from 25 to 300 °C, which were controlled using a thermocouple and a heater. The reduction effect of the employed plasma technique are discussed for different surface temperatures and compared with a thermal reducing method. The current study was performed as part of a project within the collaborative research center Oxygen-free production (SFB1368), in which several working groups investigate the influence of promising protective oxygen-free atmospheres on metal manufacturing processes like coating, welding or rolling. Within our project, we study the reduction effect of a DBD plasma in Ar/H_2 or Ar/SiH_4 mixtures on different metal systems like copper [9, 19] or iron. The further aims of the project include the implementation of the investigated DBD plasma reducing method in the industrial fabrication processes as a pre-treatment reducing step within the protective atmosphere in the system.

Materials and Methods

Samples and Preparation

Iron foils with the size of 10×10 mm^2 and a thickness of 1 mm (99.5%, Mateck GmbH, Jülich, Germany) were highly polished using a sanding machine (Jean Wirtz TG 250, Germany) with silicon carbide sanding papers and wool cloths for final diamond polishing (Struers GmbH, Hannover, Germany), resulting in smooth freshly prepared metal surfaces. After the polishing step, the samples were rinsed with ethanol (96%; Sigma-Aldrich Chemie GmbH, Munich, Germany) in an ultrasonic cleaner (Bandelin electronic GmbH & Co. KG, Berlin, Germany) for 5 min, dried and exposed to an ambient atmosphere for approximately 1 day, resulting in the formation of approximately 3 to 4 nm-thick native oxide layers [1, 22–24]. Then, the samples were analyzed via atomic force microscopy (AFM) and transferred into the ultra-high vacuum (UHV) system, where the X-ray photoelectron spectroscopy (XPS) investigations were performed [19].

Atomic Force Microscopy

The morphology and roughness of the samples before and after plasma treatments were analyzed using an Atomic Force Microscope (Dimension 3100, Veeco Instruments Inc.,

Santa Barbara, USA). The AFM images were taken in the presence of air at room temperature and atmospheric pressure. Commercial cantilevers (NSC15/Al BS, Micromasch, Wetzlar, Germany) with a spring constant of 40 N/m and a resonance frequency in the range of 325 kHz were used in the measurements. The images were recorded at a line-scan frequency of 0.5 Hz. The analysis of images was performed with the SPIP 6.1.1 software (Image Metrology, Lyngby, Denmark).

X-ray Photoelectron Spectroscopy

The chemical structure of surfaces before and after the plasma treatment was characterized via XPS at room temperature in an UHV apparatus with a base pressure of $3{\cdot}10^{-10}$ hPa using a non-monochromatic Al K_α (1486.6 eV) X–ray source (RS40B1, Prevac, Rogów, Poland). X-ray photons irradiated the surface under an angle of 80° to the surface normal, illuminating a spot with a diameter of several mm. Electrons emitted under an angle of 10° to the surface normal were recorded by a hemispherical analyzer (EA10/100, Leybold GmbH, Cologne, Germany). Survey and detailed spectra were recorded at pass energies of 80 eV and 40 eV, respectively. All XPS spectra are displayed as a function of binding energy with respect to the Fermi level. Additionally, a charge correction was applied to all spectra by referencing the C–C binding to 285.0 eV. For quantitative XPS analysis, photoelectron peak areas were calculated via a Marquardt–Levenberg optimization algorithm using CasaXPS (Casa Software Ltd., Bay House 5 Grosvenor Terrace Teignmouth, TQ14 8NE United Kingdom) with a Shirley-type background. The XPS deconvolution parameters for the detailed regions were obtained from the study on native iron oxides of Bhargava and colleagues [23]. The CasaXPS analysis files for the samples are provided in the published dataset [25].

Field Emission Scanning Electron Microscopy and Energy Dispersive *Spectroscopy*

Surface morphology and elemental composition were characterized by combined field emission scanning electron microscopy (FE-SEM) and energy dispersive spectroscopy (EDS), carried out at a Helios Nanolab 600 (FEI Germany GmbH, Frankfurt, Germany) with a dual beam system. Measurements occurred under high vacuum conditions at a base pressure of 10^{-6} hPa. Samples were attached on a standard SEM sample holder using a conductive silver liquid. SEM pictures of the sample surface were taken at an acceleration voltage of 5 kV and a probe current of 0.69 nA via an Everhart–Thornley-Detector (ETD). An X-Max 80 silicon drift detector (Oxford Instruments, Abingdon, United Kingdom) was used for EDS analysis with signals obtained at an acceleration voltage of 5 kV and 0.69 nA probe current.

Optical Emission Spectroscopy

Active species within the Ar/H_2 DBD plasma were identified via optical emission spectroscopy (OES) using an AvaSpec–ULS2048CL–EVO fiber-optic spectrometer (Avantes, Netherlands) with a measurement range of 200–1100 nm. A spectrometer was not calibrated to absolute intensity values. In order to detect the emission in the DBD plasma phase, a glass fiber was introduced into the reactor using a vacuum feedthrough (Avantes,

Netherlands). Emissions were detected in the beginning of plasma treatments at room temperature. Optical emission spectra were analysed using AvaSoft 8 (Avantes, Netherlands).

In order to study the electron temperatures of the implemented non-thermal Ar/H_2 DBD plasma, we applied the Boltzmann's plot method, which was in detail described by Das and colleagues for an Ar/H_2 non-thermal plasma [26], Falahat and colleagues for an Ar/O_2 RF DBD plasma [27] as well as in other studies [28, 29] on non-thermal Ar-based plasmas. Generally, a DBD plasma is a non-equilibrium plasma, which means that the upper energy levels of selected atomic transitions are not in the local thermodynamic equilibrium (LTE). So, the discharges in such plasmas likely do not fulfil the Maxwell–Boltzmann equilibrium and the steady-state conditions for the equations as formulated by Paris et al. [30]. However, Bonaventura and colleagues [31] proved that the equations are suited for determining accurate peak electric fields, and hence accurate peak values for average electron energies, as long as a sufficient spatial and time-integrated optical emission spectrum is used. Therefore, the Boltzmann method of analysis of electron tempeartures can still be used for the characterization of non-equilibrium plasmas with methodological assumptions and a limited reliability [27–29].

By using a set of Ar I emission lines [26, 27], which we observed with the OES (shown in the Sect. "OES study of a DBD plasma in an Ar/H2 atmosphere"), the electron temperature (T_e, in Kelvin) was estimated with Eq. (1), taking into account the measured intensity of the spectral line (I_{ik}) at the corresponding wavelength (λ_{ik}, nm) as well as the statistical weight (g_{ik}) and the probability of the electron transition (A_{ik}) from the *k*th upper ino the *i*th lower level, the upper-level excitation energy for the transition (E_k) and the Boltzmann's constant (K) [26]. The parameters as (g_{ik}), (A_{ik}) and (E_k) for each Ar I emission line were obtained from the NIST database [32]. By plotting the left part of the equation as a function of energy (E_k), we could linearly fit the obtained data and get a slope of the line that represents $\frac{1}{K \bullet T_e}$. Afterwards, the electron temperature as well as the energy could be estimated. The fitted plot and the main parameters of the observed Ar I emission lines can be found in the supplementary materials (c.f. Figure S1 and Table S1, respectively). All calculations were added to the available dataset [25].

$$ln\left(\frac{I_{ik} \bullet \lambda}{g_{ik} \bullet A_{ik}}\right) = -\frac{E_k}{K \bullet T_e} + C \tag{1}$$

DBD Plasma Reactor

The detailed description of the DBD plasma reactor was given previously in our publications on non-thermal plasma deoxidation of copper at room temperature [9, 19]. As mentioned, plasma treatment of metal samples was performed within a DBD plasma chamber that was attached to the UHV system for XPS analysis. By varying the pressure inside the reactor in the range from 10^{-8} to 10^3 hPa with an Ar/H_2 gas inlet and pump system, it was possible to treat samples at specific atmospheres and pressures and transfer them to the UHV chamber without any contact to the ambient air. For the current study a combined plasma and heat treatment was applied. Figure 1 shows a schematic representation of the setup used for DBD plasma reduction of iron surface oxides at room and elevated temperatures. A specially designed sample holder and a lift system were used during the experiments. The sample holder consists of a metal frame and the attached ceramics heater (Pyrolytic Graphite/Pyrolytic Boron Nitride type, Momentive Performance Materials Inc.,

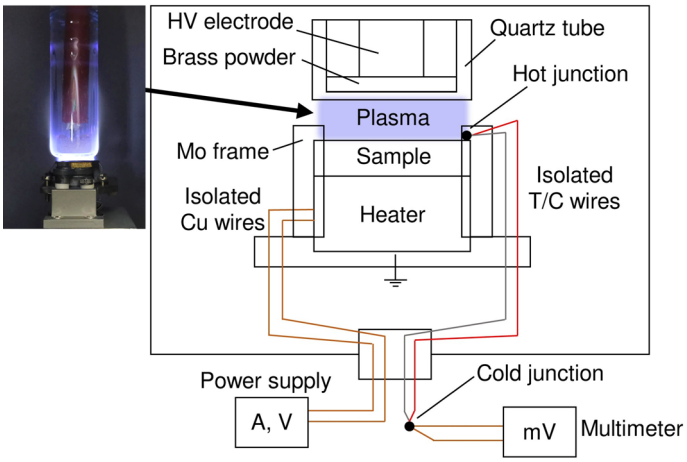

Fig. 1 Schematic representation of the experimental setup for a combined plasma and heat treatment. In addition to the schematic representation, a photo of the DBD plasma discharge in an Ar/H_2 atmosphere is presented (Color figure online)

USA) as well as a thermocouple (T/C, type C, Omega Engineering GmbH, Germany). Each iron film was placed on the ceramics heater and mounted to the holder, using a molybdenum frame. The heater was connected a power supply (Statron Ltd., Switzerland) outside the vacuum chamber using kapton-isolated copper wires and a special high vacuum feedthrough for the cables (Allectra GmbH, Germany). The control of the temperature was performed with a multimeter (Keithley Instruments Inc., USA), which was connected to the cold junction of the T/C with kapton-isolated copper wires. The cold junction was placed outside of the chamber, attached to the feedthrough and connected with the inside-placed hot junction, using two separated and isolated T/C wires. The hot junction of the T/C was placed on the surface between a sample and a molybdenum frame (calibration measurements for the thermocouple are described and presented in the supplements, c.f. Figure S2).

The DBD plasma set-up, which was applied in the current publication, was described in detail in our previous works [9, 19]. In this study, a high voltage power supply with a sinoidal output signal (PlasmaGreen GmbH, Clausthal-Zellerfeld, Germany) was used to generate 10 kV peak voltage (measured during plasma ignition, shown in the supplements, Figure S3) at 8.8 kHz pulse repetition rate for the plasma treatments. The diameter of a plasma spot was approximately 12 mm. The samples were treated at a pressure of 1000 hPa in an Ar/H_2 static atmosphere with the concentration of H_2 of 2 vol.% (Ar 4.8 and H_2 5.0, Westfalen AG, Münster, Germany) at room and elevated temperatures. The thermal treatments of samples were performed by using the same set-up without plasma treatment.

Sample Handling

Firstly, the reference state of the iron surfaces before treatment was characterized with XPS in the UHV chamber. Afterwards, the samples were transferred into the plasma reactor. An impact of thermal and plasma-thermal treatments on the oxidation state and morphologies as well as investigation of a reduction kinetics of iron surface oxides at different surface temperatures was performed by treating samples at several time intervals until an overall

time of 120 s at 1000 hPa. The heating of samples was performed at a rate of 100–150 °C per minute. As soon as the surface temperature reached a planned value, plasma treatment was started and elapsed time was measured. After the needed treatment time, the plasma as well as heating were switched off and the plasma chamber was evacuated to approximately $8{\cdot}10^{-7}$ hPa. Afterwards, the samples were transferred into the UHV chamber for XPS measurements. This process of evacuation and transfer of one sample from the plasma reactor to the UHV chamber took approximately 20 min.

Characterization of the Reduction Process

The reduction effect of a DBD plasma on iron samples at different surface temperatures was characterized by comparing the relative change in stoichiometry of the samples in relation to the reference states as determined with the XPS survey analysis. That is, the relative change in percentage (%) was calculated with the Eq. (2), taking into account the initial concentration of analysed Fe, O and C species before treatment ($n_{species(initial)}$) and the concentration of them after a treatment step ($n_{species(after)}$).

$$Relativechange = \frac{n_{species(after)} - n_{species(initial)}}{n_{species(initial)}} \bullet 100\% \tag{2}$$

Within the present study we analyzed the reduction of both Fe^{2+} and Fe^{3+} natively oxidized species by calculating the corresponding reduced fraction after each treatment step. Namely, we calculated the fraction of the sum of Fe^{2+} and Fe^{3+} components ($\nu_{species}$), according to Eq. (3), where the sum of the relative areas of the oxidized Fe^{2+} and Fe^{3+} species (a_{ox}) were divided by the sum of the relative areas of all presented iron species as Fe^0, Fe^{2+} and Fe^{3+} (a_{Fe}). The relative areas of these species were taken from the detailed Fe $2p_{3/2}$ XPS spectra.

$$\nu_{species} = \frac{a_{ox}}{a_{\mathrm{Fe}}} \tag{3}$$

Following this step, the relative reduced fraction of the sum of oxidized Fe^{2+} and Fe^{3+} species (α) was calculated with the Eq. (4), considering the initial fraction of these species before treatment ($\nu_{\text{species (initial)}}$) and after each treatment step ($\nu_{\text{species (after)}}$) [9].

$$\alpha = \frac{\nu_{species(initial)} - \nu_{species(after)}}{\nu_{species(initial)}} \tag{4}$$

Results and Discussion

Ar/H_2 Plasma Deoxidation of Iron Oxides at Different Surface Temperatures

We analyzed the effectiveness of the plasma deoxidation by comparing several iron samples that were treated with an Ar/H_2 plasma at surface temperatures ranging from 25 to 300 °C and 1000 hPa. Table 1 shows the relative changes in the stoichiometry for the natively oxidized samples that were plasma treated for 10 s at room temperature and in combination with heating. As it can be seen, plasma treatment at room temperature did not provide a strong removal of oxygen species after 10 s of treatment. Nevertheless, a pronounced

Table 1 Relative change in stoichiometry of the samples as determined with XPS for specimens treated in Ar/H_2 plasma for 10 s at different surface temperatures

Temperature (°C)	Treatment duration (s)	Relative change of concentration of species		
		Fe (%)	O (%)	C (%)
25	10	+82	−3	−51
100		+87	−7	−65
200		+235	−71	−59
300		+253	−84	−44

elimination of approximately 51% of initial carbon contaminations from the surface with an Ar/H_2 DBD plasma was observed, which is connected with the cleaning effect of the method [9, 19]. This effect could explain the relative decrease of the initial oxygen concentration of approximately 3%, which is connected with the removal of oxygen-containing organic compounds [9]. As it is shown later, plasma treatment at room temperature did not provide the oxide reduction effect even after several minutes of treatment. At the same time, we observe an increase of the effectiveness by applying additional heating treatment at temperatures from 200 to 300 °C during the plasma process, whereas plasma treatment at 100 °C did not reveal a strong increase of the deoxidation effect in comparison to room temperature treatment, which can be only associated with the removal of oxygen-containing organics. Processes at 200 °C and 300 °C provided a significant improvement, yielding a removal of oxygen species after 10 s of treatment. That is, the amount of initial oxygen species decreased by 71% and 84% after plasma treatments for 10 s at 200 °C and 300 °C, respectively. Due to the strong deoxidation effect, the concentration of observed iron species after plasma treatments at 200 °C and 300 °C was increased by a factor of approximately 3 in comparison to room temperature treatment, respectively. The high effectiveness of the cleaning effect of an Ar/H_2 plasma was in general improved at temperatures of 100 °C and 200 °C. Interestingly, the most efficient cleaning effect was observed after plasma treatment at 100 °C, whereas the application of additional heat treatment at 200 °C resulted in less productive cleaning. Moreover, treatments at the temperature of 300 °C showed the lowest impact on the concentration of carbon species. As it is shown later, the loss of effectiveness in removal of carbon contaminations at the temperatures of 200 °C and especially 300 °C is connected with the formation of additional Fe–C species on the deoxidized iron surfaces. The stoichiometry of the samples is presented in the supplements (c.f. Table S2).

Relative change in concentration of Fe and O species on the surface as a function of treatment time is presented in Fig. 2. As it can be seen, plasma treatments at room temperature and 100 °C do not provide a significant reduction of oxygen components even after two minutes of treatment. The main reason for an increase of iron species concentration after these treatments is connected with the partial removal of carbon contaminations from the surface with an Ar/H_2 plasma. In contrast, even 2 s of Ar/H_2 plasma treatment at 200 °C is enough to remove 26% of initial native oxygen species from the iron surface. Treatment for longer time brings more reduction effect, that is, 10 s plasma treatment at 200 °C results in the removal of approximately 71% of initial oxygen content. Nevertheless, treatment for 2 min did not result in a stronger deoxidation effect, yielding a removal of approximately 76% of initial oxygen species. At the same time, almost 84% of native oxygen species were reduced already after 2 s of treatment at 300 °C. Further deoxidation did not show a significant improvement, resulting in the overall deoxidation of approximately 85% of initial

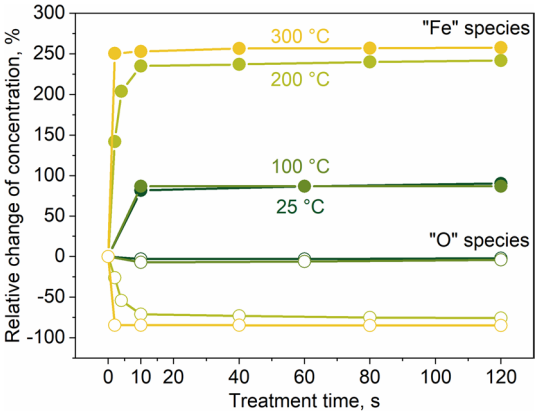

Fig. 2 Relative change of concentration of iron (solid symbol lines) and oxygen (hollow symbol lines) species as a function of treatment time for the samples during plasma treatments at 25 °C (dark green), 100 °C (green), 200 °C (light green) and 300 °C (yellow) surface temperatures (Color figure online)

oxygen species after 2 min. Residual oxygen that was presented on these samples could arise from the transportation process from the DBD chamber to the UHV chamber as well as a limited effect of the implemented treatments [9].

A detailed analysis of Fe $2p_{3/2}$, O 1s and C 1s regions was performed in order to study the chemical composition of contamination layers after treatments. Figure 3a presents the Fe $2p_{3/2}$ regions of samples after 10 s of DBD plasma treatment in an Ar/H_2 atmosphere at the surface temperatures from 25 to 300 °C (shown from bottom to top) in comparison to the reference state before treatments (bottom spectrum). The regions were studied, using the XPS deconvolution parameters from the XPS study on native iron oxides of Bhargava and colleagues [23]. We characterized the Fe $2p_{3/2}$ structure with three components as metallic iron Fe, Fe^{2+} (as for e.g. FeO) and Fe^{3+} species (like Fe_2O_3 or $Fe(OH)_3$) at 706.6, 709.1 and 711.1 eV, respectively. The relative fraction of each component for the reference state was found to be 27% (Fe), 29% (Fe^{2+}) and 44% (Fe^{3+}), so the initial native oxide layer was represented by a mixture of Fe^{2+} and Fe^{3+} oxidized species. Plasma treatments at room temperature and 100 °C for 10 s did not show a strong reduction effect, so Fe^{2+} and Fe^{3+} species were not reduced to clean Fe. However, due to the cleaning effect, an increase on

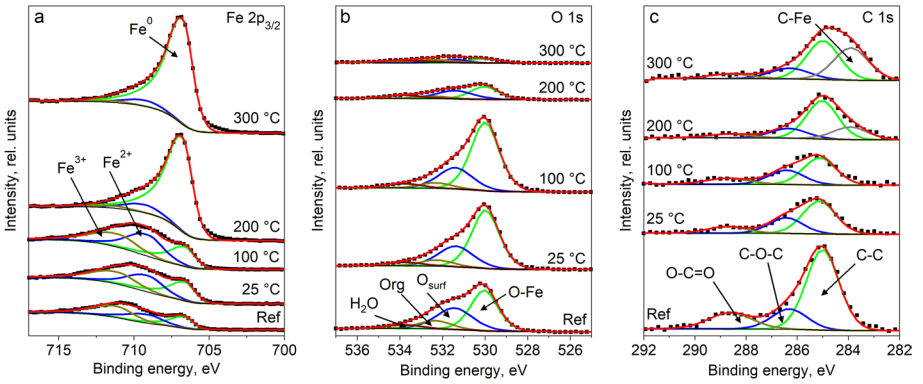

Fig. 3 **a** Fe $2p_{3/2}$, **b** O 1 s and **c** C 1 s regions of the reference sample (bottom spectra) and after 10 s treatment in an Ar/H_2 plasma at 25 °C, 100 °C, 200 °C, 300 °C surface temperatures (spectra are shown from bottom to top, respectively) (Color figure online)

intensities was detected. Nevertheless, it was observed that the Fe^{3+} species were partly reduced to Fe^{2+} species already after 10 s of plasma treatment at 25 °C and 100 °C, so the fraction of Fe^{2+} species was increased to 35% and 39%, respectively. At the same time, a sharp increase of the Fe^0 component intensity was observed after 10 s of plasma treatment at surface temperatures of 200 °C and 300 °C. So, almost no Fe^{3+} species were observed after implemented treatments, whereas the fractions of Fe^{2+} species were 9% and 6% for plasma-thermal treatments at 200 °C and 300 °C, respectively.

Figure 3b shows the O 1 s XPS region of the same samples. Generally, the spectrum of the reference sample can be deconvoluted into four peaks as iron oxide at 530.0 eV, surface oxygen species or OH^- groups at 531.4 eV, oxygen-containing organic species (e.g. C–O–C, O–C=O) at 532.6 eV as well as water at 533.8 eV [19, 23]. We observed a decrease in intensity of the components at 531.4, 532.6 and 533.8 eV after the implemented plasma treatments at 25 °C and 100 °C surface temperatures. That is, the cleaning effect as well as partial removal of surface oxygen species was observed. In contrast, an increase of an iron oxide component was detected, which could be connected with the cleaning effect and a partial oxidation of iron surfaces at low temperatures. In contrast, we observed a considerable reduction of all oxygen components after 10 s plasma treatments at elevated surface temperatures of 200 °C and 300 °C.

Figure 3c represents the C 1 s XPS regions of these samples. The reference state was characterized by C–C, C–O–C and O–C=O species at 285.0 eV, 286.3 eV and 288.6 eV, respectively [9, 23]. After plasma treatment at room temperature and 100 °C for 10 s we observed a strong decrease of all components, pointing towards a considerable cleaning effect of an Ar/H_2 plasma. The C 1s regions of the samples after 10 s treatments at elevated surface temperatures of 200 °C and 300 °C are represented by almost the same structures with the addition of a component at the binding energy of approximately 283.8 eV. These species were assigned to the C–Fe bond [33–35], which could be formed during deoxidation and additional heating of iron samples. Due to the close values in binding energies of Fe–Fe and Fe–C species within the Fe $2p_{3/2}$ region (the difference between the peaks is approximately 0.7 eV [23, 33]), we were not able to precisely separate them. Therefore, the Fe–C component was not introduced into the final Fe $2p_{3/2}$ fits. Generally, all the detailed XPS deconvolution parameters of the observed components can be found in the supplements in the Table S3.

Morphology of Treated Surfaces

The analysis of the sample morphology before and after plasma treatments at different surface temperatures is presented in Fig. 4. The analysis of the samples was performed in comparison to the reference state (c.f. Figure 4a) in the presence of air after reoxidation of treated samples for approximately one day. That is, Ar/H_2 plasma treatment at room temperature and 100 °C did not result in a strong impact on the surface morphology even after 2 min of treatment (c.f. Figure 4b and c), which was also observed in our studies [9, 19]. As discussed previously, plasma treatments at 25 °C and 100 °C only provided a cleaning effect, but no reduction or formation of other compounds were observed with the XPS method on the surfaces after 120 s of plasma treatments at 25 °C and 100 °C. In contrast, the surfaces of the samples after plasma-thermal treatments at elevated temperatures of 200 °C and 300 °C were found to be mottled with round-shaped structures (c.f. Figure 4e–i). Those structures could be assigned to the Fe–C component that was observed with the XPS analysis of these samples after 10 s as well as after 120 s of

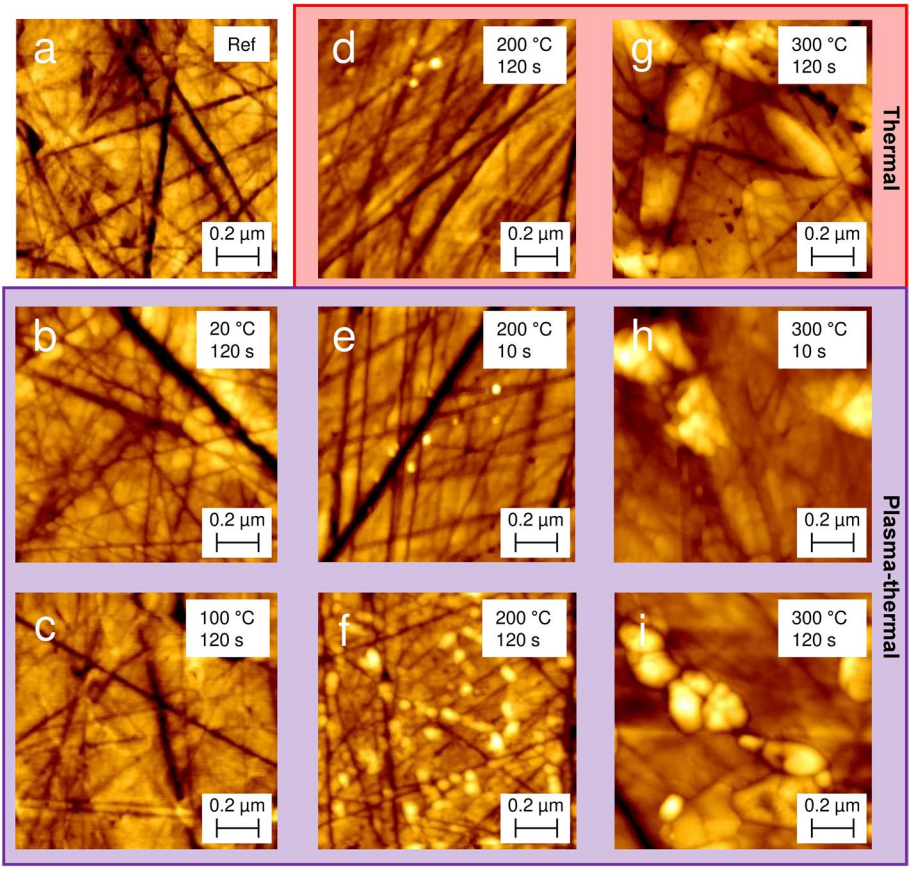

Fig. 4 AFM images of the reference sample (**a**) and samples after Ar/H_2 plasma-thermal treatment at 25 °C (**b**), 100 °C (**c**), 200 °C (**e**, **f**), 300 °C (**h**, **i**) surface temperatures. In addition, the samples after thermal treatment at 200 °C (**d**) and 300 °C (**g**) are presented. The scan size is 1 µm × 1 µm (Color figure online)

treatment. The amount of particles on the surfaces increases with longer treatment time. That is, the surface of the sample after 10 s of plasma-thermal treatment at 200 °C was covered with barely visible and infrequent structures of approximately 40–60 nm in diameter (c.f. Figure 4e). For a longer treatment time of 120 s the size and amount of particles were increased (c.f. Figure 4f), which was observed with the AFM as well as XPS, as it is presented later in the Sect. "Comparison of thermal and plasma-thermal reduction". That is, 120 s of plasma-thermal treatment at 200 °C resulted in the formation of approximately 9 nm-thick particles with a diameter of approximately 50 to 80 nm. Interestingly, the size of structures increased with the rise of the surface temperature. The sample after 10 s of plasma treatment at 300 °C contained approximately 10 to 15-nm-thick clusters of 150–300 nm in diameter (c.f. Figure 4h), the amount of which grew after treatment for 120 s (c.f. Figure 4i) (the surface plots for the discussion of the thickness of particles are presented in the supplements, Figure S4).

The formation of Fe–C structures was also detected on the samples after 120 s of heating treatment in an Ar/H_2 atmosphere without plasma exposure (c.f. Figure 4d and g). After 120 s of thermal treatment at 200 °C (c.f. Figure 4d), we observed barely visible 50 nm structures on the surface that have approximately the same sizes as for the combined plasma-thermal treatment at 200 °C for 10 s (c.f. Figure 4e). In contrast, the sample after thermal treatment at 300 °C showed inhomogeneous morphology with the 150–300 nm structures that protrude from the material. Such effect could be connected with the thermally driven diffusion of the carbon bulk contaminations to the deoxidized iron surface [36, 37]. As it is discussed later in the Sect. "Comparison of thermal and plasma-thermal reduction", thermal treatment does not result in the significant removal of adventitious carbon contaminations, but even more C–C components were observed, which hints to carbon diffusion towards the surface. Generally, these clusters have almost the same size as after combined plasma-thermal treatment at the same temperature. Nevertheless, we observed more Fe–C species on the surface after plasma-thermal treatment (as it is shown later with XPS method, c.f. Figure 7) that is probably connected with the additional reaction between the plasma-activated carbon species from the destroyed C–C, C–O–C, O–C=O surface structures with the deoxidized iron surfaces [37, 38].

Figure 5 depicts the scanning electron microscopy (SEM) images of the reference iron surface (a) and samples after plasma-thermal treatments for 120 s at 200 °C (b) and 300 °C (c). The reference sample features a smooth structure without any visible particles. In contrast, as it was observed with the AFM, the plasma-thermal treated surfaces contained particles of approximately 50 nm and 200 nm in diameter for the experiments at 200 °C and 300 °C, respectively. We performed the energy dispersive spectroscopy (EDS) in order to study the differences in morphology and the elemental composition of the particles. Distinct differences in the quantity of observed elements was detected for the surface after plasma-thermal treatment at 300 °C with bigger particles (c). We measured several spots on the surface that contained particles as well as only the substrate (c.f. Figure 5c, the measurement spots are highlighted with red in the inlay). Importantly, we observed higher amounts of carbon species on the measured structures in comparison to the iron substrate. Namely, the particles contained approximately 16 at.% of C and 84 at.% of Fe, whereas the substrate was characterized by 3 at.% of C and 97 at.% of Fe. Smaller differences were obtained for the sample after plasma-thermal treatment at 200 °C with 50-nm structures on the surface. Due to the known limitations in information depth and lateral resolution of EDS [39], we were not able to characterize

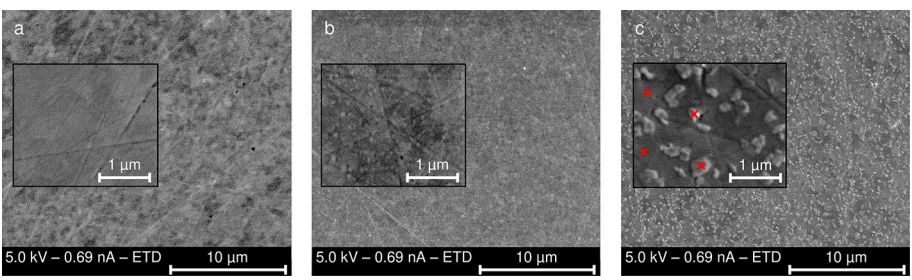

Fig. 5 SEM images of the reference sample (**a**) and samples after 120 s of Ar/H_2 plasma-thermal treatment at surface temperatures of 200 °C (**b**) and 300 °C (**c**) (Color figure online)

the exact composition of particles, despite reducing the acceleration voltage down to 5 kV. Nevertheless, the observed differences allowed us to assume, that these particles could represent the Fe–C structures that were detected with the XPS method previously. The EDS analysis as well as the exact measurement spots are presented in the supplements (Figure S5, S6 and Table S4, S5).

Comparison of Thermal and Plasma-Thermal Reduction

Figure 6 shows the time-dependent reduction of natively oxidized species of iron as Fe^{2+} and Fe^{3+} during combined plasma-thermal (blue color) and thermal (red color) treatments at 200 °C in an Ar/H_2 atmosphere at 1000 hPa. It indicates that an almost complete reduction of Fe^{2+} and Fe^{3+} species was obtained in both cases with differences in efficiency. That is, a plasma-thermal method results in the reduction of ~ 84% of initial oxidized species after approximately 10 s and reaches the maximum value of ~ 88% after approximately 80 s. In contrast, thermal treatment for 10 s resulted in the conversion of approximately 22% of initial oxidized species, whereas an almost full reduction of ~ 86% was obtained after approximately 300 s. The increase in reduction efficiency of oxidized Fe^{2+} and Fe^{3+} components, which we observed for combined plasma-thermal treatment in comparison to the thermal reduction, can certainly be attributed to highly reactive atomic hydrogen species [9] (shown later in the Sect. "OES study of a DBD plasma in an Ar/H2 atmosphere") and most probably other reducing agents like vibrationally excited hydrogen molecules, which were found to be present in non-thermal plasmas [5]. It is known that the presence of such hydrogen species within the system stimulates the reduction process due to the higher reactivity in comparison to neutral H_2 species as well as the factors of their recombination, dissociation and diffusion into the crystal structure [5]. Interestingly, we observed almost no differences in the reduction efficiencies of thermal and plasma-thermal treatments at 300 °C on thin native layers (c.f. Figure S7, in supplements). So, both treatments resulted in the reduction of approximately ~ 91% of intial Fe^{2+} and Fe^{3+} oxidized species already after 10 s.

The C 1s XPS regions of the samples after several steps of thermal (a) and plasma-thermal (b) treatments at the surface temperature of 200 °C are presented in the Fig. 7. We observed that thermal treatment at the temperature of 200 °C did not result in the significant reduction of adventitious carbon contaminations, which were represented in the XPS spectra by C–C (285.0 eV), C–O–C (286.3 eV) and O–C=O (288.6 eV) structures [23]. In

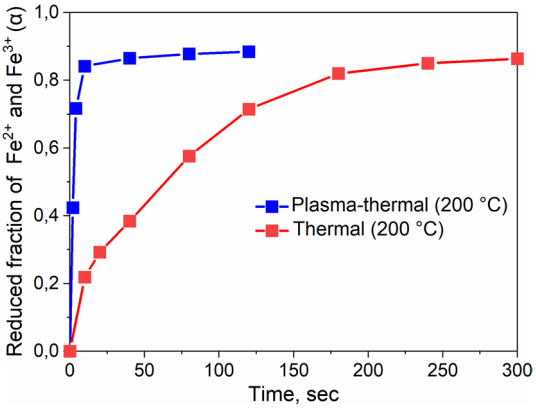

Fig. 6 Isotherms of reduction of Fe^{2+} and Fe^{3+} species as a function of treatment time. Experimental data for the plasma-thermal (blue symbols) and thermal (red symbols) treatments at 200 °C is presented (Color figure online)

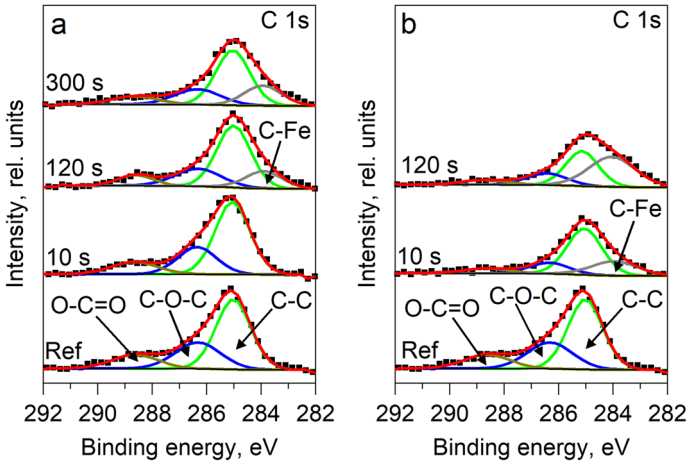

Fig. 7 C 1 s region of the samples after several steps of thermal (**a**) and plasma-thermal (**b**) treatments at 200 °C (Color figure online)

contrast, we observed a cleaning effect by applying an Ar/H_2 DBD plasma at the same surface temperature. That is, almost full removal of oxidized carbon contaminations as well as partial reduction of C–C structures were detected already after 10 s of plasma-thermal treatment. Concurrent, formation of C–Fe components was revealed for both treatments with the difference in the time of appearance as well as amount of species. So, C–Fe structures were detected on surfaces after approximately 80 s to 120 s of thermal treatment and 10 s of plasma-thermal treatment. The formation of such components appears to be related to the process of deoxidation of iron metal [37] that, as discussed previously, was almost fully obtained also after approximately 80 s to 120 s for thermal and 10 s for plasma-thermal treatments. The higher amount of the detected C–Fe structures on the deoxidized surfaces, which was observed for the plasma-thermal experiment (after 120 s) in comparison to the thermal one (after 300 s), is probably related to a degradation of carbon surface species by the Ar/H_2 plasma. Whereas thermal treatment most probably did not provide a significant destruction of surface carbon contaminations but could result in the thermal diffusion of carbon bulk contaminations to the metal [36, 37, 40], an additional non-thermal Ar/H_2 plasma could result in the destruction of surface adventitious carbon species that probably directly react with the deoxidized Fe [37].

OES Study of a DBD Plasma in an Ar/H_2 Atmosphere

The reactive species as well as the electron temperature within the implemented plasma phase in an Ar/H_2 atmosphere at 1000 hPa were characterized with the OES. Figure 8 shows an OES spectrum of the DBD Ar/H_2 plasma. In the present case, we observed highly intense emission peaks of Ar I species in the region from 696 to 965 nm. These lines were used to estimate the electron temperature with the Boltzmann method (c.f. Sect. "Optical Emission Spectroscopy"). That is, the calculated T_e was found to be ~ 8400 K or ~ 0.7 eV, which is close to the typical T_e of nonthermal plasma systems [5, 26]. In addition to Ar I lines, the low intensity emissions from atomic hydrogen species H_α at approximately 656.5 nm were detected [9]. Because of the weak radiation throughout the spectra,

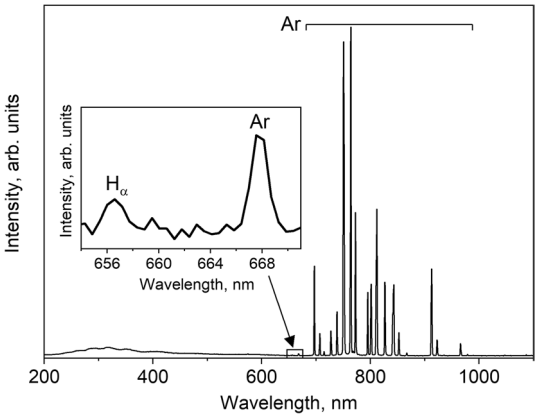

Fig. 8 OES spectrum of an Ar/H_2 DBD plasma at 1000 hPa and 25 °C

hydrogen lines are commonly characterized by low intensities in hydrogen-contained plasmas [9, 41]. Nonetheless, such low intensity observations still clearly confirm the existence of the hydrogen species in the plasma [9, 41]. That is, we can assume that the presence of atomic hydrogen increases the metal reduction effectiveness of the implemented DBD Ar/H_2 plasma, which was also discussed in other publications on non-thermal hydrogen reducing plasmas [9, 12, 20, 42]. In addition, based on the calculated electron temperature, we could assume the existence of further highly reactive species like excited-state hydrogen molecules within the plasma phase [5, 43]. Unfortunately, the emissions of these species can not be directly observed with the OES method. Nevertheless, according to several studies, the electron temperature of non-thermal plasmas of approximately 1 eV is enough for the generation of vibrationally excited hydrogen molecules, which are assumed to play a crucial role in the reduction of metal oxides with non-thermal hydrogen plasmas [5, 13, 43]. Moreover, a broad emission in the range from 200 to approximately 400 nm was detected, which could be explained by two factors as the dissociation continuum from H_2 molecules in argon gas [44] or by the photoluminescence effect, which was also observed for the Ar/H_2 radio-frequency plasmas by Lebreton and colleagues [45]. Besides the main components, a low-intensity emission peak at ~ 667.5 nm was observed, which could be assigned to Ar I species. Other contaminants like water or organics were not detected.

Conclusions

A dielectric barrier discharge plasma was applied for the reduction of natively oxidized iron surfaces in an Ar/H_2 atmosphere at 1000 hPa and different surface temperatures. The results reveal that oxidized Fe^{2+} and Fe^{3+} species can be almost fully reduced to clean metal after approximately 10 s of combined plasma-thermal treatment at 200 °C and 300 °C, whereas plasma treatment at room temperature results only in the significant removal of adventitious carbon contaminations. By comparing the plasma-thermal and thermal treatments, we observe an increase in the reduction efficiency for the plasma treatment at the surface temperature of 200 °C. In particular, the plasma-thermal method at 200 °C results in the reduction of ~ 84% of the initial oxidized iron species after 10 s with obtaining its maximum of ~ 88% after approximately 80 s of treatment. At the same time, thermal reduction results in the conversion of only 22% of the Fe^{2+} and Fe^{3+} species after

10 s and ~ 86% after 300 s. We show that the origin of the high reducing efficiency of a studied Ar/H_2 DBD plasma is most probably due to the presence of atomic hydrogen species in the plasma phase. Additionally, the estimated electron temperatures hints towards a probable presence of other highly reactive species like rovibrationally excited hydrogen molecules that also stimulate the reduction process.

The AFM analysis of morphology of the treated samples after reoxidation in air reveal that plasma treatment at room temperature does not provide observable changes to the surface structure, whereas thermal and plasma-thermal treatments at elevated temperatures of 200 °C and 300 °C result in the formation of additional clusters on the surface. We attribute the observed particles to the Fe–C structures, the presence of which was detected with the XPS as well as EDS methods. The amount of particles is increased with the longer treatment time, and may hence be connected with the higher reduced fraction of a Fe metal over time. The sizes of particles depend on the surface temperature. Namely, the surfaces after treatments at 200 °C contain ~ 50 nm structures, whereas treatments at 300 °C result in the formation of ~ 150–300 nm clusters.

Supplementary Information The online version contains supplementary material available at https://doi.org/10.1007/s11090-023-10346-7.

Acknowledgements The project was funded by the Deutsche Forschungsgemeinschaft (DFG, German Research Foundation) – Project-ID 394563137 – SFB1368.

Author's Contribution VU: Conceptualization, Formal analysis, Investigation, Data Curation, Writing—Original Draft, Visualization. LW: Conceptualization, Writing—Original Draft. M.S: Investigation, Writing—Original Draft. SD: Conceptualization, Formal analysis, Data Curation, Writing—Original Draft, Funding acquisition. R.G: Project administration, Funding acquisition. WM-F: Conceptualization, Resources, Writing—Review & Editing, Supervision, Project administration, Funding acquisition.

Funding Open Access funding enabled and organized by Projekt DEAL.

Data Availability All raw and analyzed data have been made available through Zenodo at https://doi.org/10.5281/zenodo.7369268.

Declarations

Conflict of interest The authors have no relevant financial or non-financial interest to disclose.

References

1. Wendel J, Manchili SK, Hryha E et al (2020) Reduction of surface oxide layers on water-atomized iron and steel powder in hydrogen: effect of alloying elements and initial powder state. Thermochim Acta 692:178731. https://doi.org/10.1016/j.tca.2020.178731
2. Chasoglou D, Hryha E, Nyborg L (2013) Effect of process parameters on surface oxides on chromium-alloyed steel powder during sintering. Mater Chem Phys 138:405–415. https://doi.org/10.1016/j.matchemphys.2012.11.074

3. Spreitzer D, Schenk J (2019) Reduction of iron oxides with hydrogen—a review. Steel Res Int 90:1900108. https://doi.org/10.1002/srin.201900108
4. Ardelean E, Socalici A, Ardelean M et al (2017) The analysis of the steel deoxidation process in a vacuum installation. IOP Conf Ser Mater Sci Eng 163:12025. https://doi.org/10.1088/1757-899X/163/1/012025
5. Sabat KC, Murphy AB (2017) Hydrogen plasma processing of iron ore. Metall Mater Trans B 48:1561–1594. https://doi.org/10.1007/s11663-017-0957-1
6. Sawada Y, Ogawa S, Kogoma M (1995) A new approach to the copper/epoxy joint using atmospheric pressure glow discharge. J Adhes 53:173–182. https://doi.org/10.1080/00218469508009937
7. Eustathopoulos N, Sobczak N, Passerone A et al (2005) Measurement of contact angle and work of adhesion at high temperature. J Mater Sci 40:2271–2280. https://doi.org/10.1007/s10853-005-1945-4
8. Sabat KC, Rajput P, Paramguru RK et al (2014) Reduction of oxide minerals by hydrogen plasma: an overview. Plasma Chem Plasma Process 34:1–23. https://doi.org/10.1007/s11090-013-9484-2
9. Udachin V, Wegewitz L, Dahle S et al (2022) Reduction of copper surface oxide using a sub-atmospheric dielectric barrier discharge plasma. Appl Surf Sci 573:151568. https://doi.org/10.1016/j.apsusc.2021.151568
10. Upadhya K, Moore JJ, Reid KJ (1984) Application of plasma technology in iron and steelmaking. JOM 36:46–56. https://doi.org/10.1007/BF03339937
11. Vepřek S, Patscheider J, Elmer J (1985) Restoration and conservation of ancient artifacts: a new area of application of plasma chemistry. Plasma Chem Plasma Process 5:201–209. https://doi.org/10.1007/BF00566215
12. Ramos SV, Cisquini P, Nascimento RC Jr et al (2021) Morphological changes and kinetic assessment of Cu_2O powder reduction by non-thermal hydrogen plasma. J Market Res 11:328–341. https://doi.org/10.1016/j.jmrt.2020.12.038
13. Rajput P, Bhoi B, Sahoo S et al (2013) Preliminary investigation into direct reduction of iron in low temperature hydrogen plasma. Ironmaking Steelmaking 40:61–68. https://doi.org/10.1179/174328121212Y.0000000023
14. Mozetič M, Zalar A, Drobnič M (1999) Reduction of thin oxide layer on Fe60Ni40 substrates in hydrogen plasmas. Thin Solid Films 343–344:101–104. https://doi.org/10.1016/S0040-6090(98)01621-6
15. Huczko A, Meubus P (1988) Vapor phase reduction of chromic oxide in an Ar-H_2 Rf plasma. Metall Mater Trans B 19:927–933. https://doi.org/10.1007/BF02651415
16. Huczko A, Meubus P (1989) Vapor phase hydrogen reduction of chromic oxide in an RF plasma. Z Phys Chem 270(1):561–568. https://doi.org/10.1515/zpch-1989-27066
17. Ogorodnikova OV, Zhou Z, Sugiyama K et al (2017) Surface modification and deuterium retention in reduced-activation steels under low-energy deuterium plasma exposure. Part I: undamaged steels. Nucl Fusion 57:36010. https://doi.org/10.1088/1741-4326/57/3/036010
18. Mozetič M, Vesel A, Kovač J et al (2015) Formation and reduction of thin oxide films on a stainless steel surface upon subsequent treatments with oxygen and hydrogen plasma. Thin Solid Films 591:186–193. https://doi.org/10.1016/j.tsf.2015.02.007
19. Udachin V, Wegewitz L, Dahle S et al (2022) Dielectric barrier discharge plasma deoxidation of copper surfaces in an Ar/SiH4 atmosphere. Plasma Chem Plasma Process. https://doi.org/10.1007/s11090-022-10268-w
20. Sawada Y, Taguchi N, Tachibana K (1999) Reduction of copper oxide thin films with hydrogen plasma generated by a Dielectric-Barrier glow discharge. Jpn J Appl Phys 38:6506–6511. https://doi.org/10.1143/JJAP.38.6506
21. Xu ZJ, Qi B, Di LB (2013) On the mechanism of copper oxide reduction by dielectric barrier discharge plasma using H_2 and Ar mixture gases. AMR 690–693:1664–1667. https://doi.org/10.4028/www.scientific.net/AMR.690-693.1664
22. Suzuki S, Ishikawa Y, Isshiki M et al (1997) Native oxide layers formed on the surface of ultra high-purity iron and copper investigated by angle resolved XPS. Mater Trans JIM 38:1004–1009. https://doi.org/10.2320/matertrans1989.38.1004
23. Bhargava G, Gouzman I, Chun CM et al (2007) Characterization of the "native" surface thin film on pure polycrystalline iron: a high resolution XPS and TEM study. Appl Surf Sci 253:4322–4329. https://doi.org/10.1016/j.apsusc.2006.09.047
24. Grosvenor AP, Kobe BA, McIntyre NS et al (2004) Use of QUASES™/XPS measurements to determine the oxide composition and thickness on an iron substrate. Surf Interface Anal 36:632–639. https://doi.org/10.1002/sia.1842
25. Udachin V, Wegewitz L, Szafarska M et al (2022) Raw and analyzed data for manuscript "Atmospheric non-thermal plasma reduction of natively oxidized iron surfaces." Zenodo 1:1. https://doi.org/10.5281/zenodo.7369268

26. Das S, Das DP, Sarangi CK et al (2018) Optical emission spectroscopy study of Ar–H_2 plasma at atmospheric pressure. IEEE Trans Plasma Sci 46:2909–2915. https://doi.org/10.1109/TPS.2018.2850855
27. Falahat A, Ganjovi A, Taraz M et al (2018) Optical characteristics of a RF DBD plasma jet in various Ar/O_2 mixtures. Pramana J Phys 90:27. https://doi.org/10.1007/s12043-018-1520-6
28. Subedi DP, Shrestha R, Tyata RB et al (2017) Generation and diagnostics of atmospheric pressure dielectric barrier discharge in argon/air. Indian J Pure Appl Phys (IJPAP) 55:155–162
29. Akatsuka H (2019) Optical Emission Spectroscopic (OES) analysis for diagnostics of electron density and temperature in non-equilibrium argon plasma based on collisional-radiative model. Adv Phys X 4:1592707. https://doi.org/10.1080/23746149.2019.1592707
30. Paris P, Aints M, Valk F et al (2005) Intensity ratio of spectral bands of nitrogen as a measure of electric field strength in plasmas. J Phys D Appl Phys 38:3894–3899. https://doi.org/10.1088/0022-3727/38/21/010
31. Bonaventura Z, Bourdon A, Celestin S et al (2011) Electric field determination in streamer discharges in air at atmospheric pressure. Plasma Sources Sci Technol 20:35012. https://doi.org/10.1088/0963-0252/20/3/035012
32. Kramida A, Ralchenko Y (1999) NIST Atomic Spectra Database, NIST Standard Reference Database 78. National Institute of Standards and Technology
33. Tian Z, Wang C, Yue J et al (2019) Effect of a potassium promoter on the Fischer–Tropsch synthesis of light olefins over iron carbide catalysts encapsulated in graphene-like carbon. Catal Sci Technol 9:2728–2741. https://doi.org/10.1039/C9CY00403C
34. Lee H, Lee W-J, Park Y-K et al (2018) Liquid phase plasma synthesis of iron oxide nanoparticles on nitrogen-doped activated carbon resulting in nanocomposite for supercapacitor applications. Nanomaterials (Basel) 8:190. https://doi.org/10.3390/nano8040190
35. Yang C, Zhao H, Hou Y et al (2012) Fe_5C_2 nanoparticles: a facile bromide-induced synthesis and as an active phase for Fischer–Tropsch synthesis. J Am Chem Soc 134:15814–15821. https://doi.org/10.1021/ja305048p
36. Arai T (2015) The thermo-reactive deposition and diffusion process for coating steels to improve wear resistance. Thermochemical Surface Engineering of Steels. Elsevier, pp 703–735. https://doi.org/10.1533/9780857096524.5.703
37. Aguiló-Aguayo N, Liu Z, Bertran E et al (2013) Thermal-induced structural evolution of carbon-encapsulated iron nanoparticles generated by two different methods. J Phys Chem C 117:19167–19174. https://doi.org/10.1021/jp4025552
38. Zhao H, Liu J-X, Yang C, Yao S, Hai-Yan S, Gao Z, Dong M, Wang J, Rykov AI, Wang J, Hou Y, Li W-X, Ma D (2021) Synthesis of iron-carbide nanoparticles: identification of the active phase and mechanism of Fe-based Fischer–Tropsch synthesis. CCS Chem 3(11):2712–2724. https://doi.org/10.31635/ccschem.020.202000555
39. Linke R, Schreiner M, Demortier G et al (2003) Determination of the provenance of medieval silver coins: potential and limitations of x-ray analysis using photons, electrons or protons. X-ray Specttom 32:373–380. https://doi.org/10.1002/xrs.654
40. Rodríguez DG, Gleeson MA, Lauritsen JV et al (2022) Iron carbide formation on thin iron films grown on Cu(1 0 0): FCC iron stabilized by a stable surface carbide. Appl Surf Sci 585:152684. https://doi.org/10.1016/j.apsusc.2022.152684
41. Saboohi S, Griesser HJ, Coad BR et al (2018) Promiscuous hydrogen in polymerising plasmas. Phys Chem Chem Phys 20:7033–7042. https://doi.org/10.1039/c7cp08166a
42. Prysiazhnyi V, Brablec A, Čech J et al (2014) Generation of large-area highly-nonequlibrium plasma in pure hydrogen at atmospheric pressure. Contrib Plasma Phys 54:138–144. https://doi.org/10.1002/ctpp.201310060
43. Di L, Zhang X, Xu Z (2014) Preparation of copper nanoparticles using dielectric barrier discharge at atmospheric pressure and its mechanism. Plasma Sci Technol 16:41–44. https://doi.org/10.1088/1009-0630/16/1/09
44. Lavrov BP, Melnikov AS, Käning M et al (1999) UV continuum emission and diagnostics of hydrogen-containing nonequilibrium plasmas. Phys Rev E 59:3526–3543. https://doi.org/10.1103/PhysRevE.59.3526
45. Lebreton F, Abolmasov SN, Silva F et al (2016) In situ photoluminescence study of plasma-induced damage at the a –Si:H/c–Si interface. Appl Phys Lett 108:51603. https://doi.org/10.1063/1.4941298